JOURNAL OF GUIDANCE, CONTROL, AND DYNAMICS
Vol. 33, No. 1, January–February 2010

Verifiable Adaptive Flight Control: Unmanned Combat Aerial Vehicle and Aerial Refueling

Jiang Wang*
Virginia Polytechnic Institute and State University, Blacksburg, Virginia 24061
Naira Hovakimyan†
University of Illinois at Urbana-Champaign, Urbana, Illinois 61801
and
Chengyu Cao‡
University of Connecticut, Storrs, Connecticut 06269

DOI: 10.2514/1.45330

This paper presents the $\mathcal{L}_1$ adaptive controller for two benchmark flight control applications. The benefit of the proposed adaptive control approach is its promise for development of theoretically justified tools for verification and validation of adaptive systems. It has a priori predictable performance bounds and a guaranteed bounded-away-from-zero, time-delay margin in the presence of fast adaptation. Two flight control examples, unmanned combat aerial vehicle and aerial refueling autopilot, are considered in the presence of nonlinear uncertainties and control surface failures. The $\mathcal{L}_1$ adaptive controller without any redesign leads to a scaled response for the system input and output signals, dependent upon changes in the initial conditions, the reference inputs, and the uncertainties.

I. Introduction

SINCE the early 1990s, the U.S. Air Force, the U.S. Navy, and NASA, in collaboration with industry and academia, have made significant progress toward maturing the adaptive control theory for application to reconfigurable/damage adaptive flight control for aircraft and weapons systems. Reconfigurable flight control refers to the ability of a flight control system to adapt to unknown failures, damage, and uncertain aerodynamics. Flight control systems that are adaptive and reconfigurable constitute an important element in the design of mission-effective unmanned combat systems. These properties of the control system can increase the reliability of unmanned systems.

Both indirect and direct adaptive control methods have been investigated, and several approaches have been successfully flown on manned and unmanned aircraft, and also on advanced weapon systems. Indirect adaptive-based approaches include the self-repairing flight control systems, the self-designing controller, and the Intelligent Flight Control System: Generation I. Direct adaptive control-based approaches have been successfully used in the Reconfigurable Control for Tailless Fighters (RESTORE) program. The application of those technologies under the RESTORE program led to the flight testing of the approach on the Boeing/NASA X-36 agility research test aircraft. Success in the RESTORE dynamic inversion-based adaptive control of aircraft and missiles offered the potential to develop flight control systems without knowledge of the aerodynamics. These technological advances paved the road to successful transition of adaptive flight control methods into two Boeing/U.S. Air Force production programs [1–4].

The results in [5–7] demonstrated the benefits and the potential of direct adaptive control for flying vehicles. The challenges and the open problems in this direction were summarized in [8]. The recently developed $\mathcal{L}_1$ adaptive controller addressed some of those challenges by establishing a new paradigm for design of adaptive control systems with analytically provable performance/robustness guarantees. The key feature of the $\mathcal{L}_1$ adaptive controller is that it achieves separation between adaptation and robustness and replaces the tuning of the (adaptation) rate of the nonlinear gradient minimization scheme (governing the adaptive law) by design of a low-pass filter that can be addressed using tools from the linear systems theory and robust control. The $\mathcal{L}_1$ adaptive control methodology for the first time enables design of a nonlinear closed-loop control system with a guaranteed, analytically provable, bounded-away-from-zero time-delay margin in the presence of fast adaptation [9,10]. Its guaranteed performance bounds and systematic design procedure can significantly reduce the control system development time in an industrial setting. The performance limitations of the $\mathcal{L}_1$ adaptive controller are shown to be consistent with hardware limitations (CPU and control channel bandwidth). Furthermore, its ability of fast adaptation allows for control of nonlinear systems by adapting two parameters only [11]. This, in particular, eliminates the need for selecting and tuning neural network basis functions, which typically has been one of the major issues in the architecture. These features of the $\mathcal{L}_1$ adaptive controller lay the foundation for the development of theoretically justified tools for validation and verification (VV) of adaptive systems. Briefly, its features (as proven in [9–14]) can be summarized as 1) guaranteed fast adaptation, limited only by available hardware (CPU); 2) decoupling between adaptation and robustness; guaranteed transient performance for system input and output signals; 3) guaranteed transient performance for system input and output signals; 4) guaranteed and bounded-away-from-zero time-delay margin in the presence of fast adaptation; and 5) uniform scaled transient response, dependent on changes in initial conditions, uncertainties, and reference commands.

We present the $\mathcal{L}_1$ adaptive controller for two benchmark examples of flight control. First, the X-45A unmanned combat aerial vehicle (UCAV) in the presence of unknown control effectiveness reduction and pitching moment uncertainty is discussed. Simulation results demonstrate the benefits of the $\mathcal{L}_1$ adaptive controller. The time-delay margin is computed and shown to be consistent with the

Presented as Paper 6658 at the AIAA Guidance, Navigation, and Control Conference and Exhibit, Honolulu, HI, 18–21 August 2008; received 7 May 2009; revision received 29 September 2009; accepted for publication 2 October 2009.

*Graduate Research Assistant, Department of Aerospace and Ocean Engineering, 215 Randolph Hall; jwang005@vt.edu. Student Member AIAA (Corresponding Author).

†Professor, Department of Mechanical Science and Engineering; nhovakim@illinois.edu. Associate Fellow AIAA.

‡Research Assistant Professor, Department of Mechanical Engineering; ccao@engr.uconn.edu. Member AIAA.

theoretical predictions. Next, the autonomous aerial refueling (AAR) problem is considered in the presence of vortex-induced uncertainties. The simulation is done using Barron Associates' tailless aircraft model [15]. In both applications, a single design of the $\mathcal{L}_1$ adaptive controller achieves (guaranteed) scaled response for both system signals, dependent upon changes in the initial conditions, the reference inputs, and the system uncertainties.

II. Problem Formulation

The adaptive flight control architecture in this paper includes a fixed-gain robust baseline controller and an augmentation of it by an adaptive increment. The baseline controller is designed to yield consistent nominal system performance in the absence of failures, whereas the adaptive element provides adaptation and reconfiguration in the presence of system uncertainties (e.g., battle damage), control failures, and unknown aerodynamics. The linearized open-loop plant dynamics, used in the design of a baseline controller, can be generalized and written in the form:

$$\begin{cases} \dot{x}_p(t) = A_p x_p(t) + B_p \Lambda\{u(t) + K_0[t, x_p(t)]\}, \quad x_p(0) = x_{p_0} \\ y(t) = C_p x_p(t) + D_p \Lambda\{u(t) + K_0[t, x_p(t)]\} \\ z_p(t) = F y(t) \end{cases} \tag{1}$$

where $A_p \in \mathbb{R}^{n_1 \times n_1}$, $B_p \in \mathbb{R}^{n_1 \times m}$, $C_p \in \mathbb{R}^{l \times n_1}$, $D_p \in \mathbb{R}^{l \times m}$, and $F \in \mathbb{R}^{p \times l}$ are known matrices; $u(t) \in \mathbb{R}^m$ is the virtual control input; the diagonal matrix $\Lambda \in \mathbb{R}^{m \times m}$ is unknown with strictly positive diagonal elements Λ_i; $i = 1, 2, \cdots, m$, which models failures in control effectiveness; and $K_0(t, x_p) \in \mathbb{R}^m$ is the unknown nonlinear function of the system states. The output $y(t)$ represents the sensor measurements, and $z_p(t)$ is a subset of the plant outputs to be regulated.

The dynamics of the baseline controller can be generalized and written in the form:

$$\begin{cases} \dot{x}_c(t) = A_c x_c(t) + B_{1c} z_c(t) + B_{2c} z_p(t) \\ u(t) = C_c x_c(t) + D_{1c} z_c(t) + D_{2c} z_p(t) \end{cases} \tag{2}$$

where $z_c(t) \in \mathbb{R}^q$ is the vector of the outer-loop commands from guidance, and $x_c \in \mathbb{R}^{n_2}$. Substituting $z_p(t)$ from Eq. (1) into Eq. (2) yields

$$\begin{cases} \dot{x}_c(t) = A_c x_c(t) + B_{1c} z_c(t) + B_{2c} F(C_p x_p(t) + D_p \Lambda\{u(t) + K_0[t, x_p(t)]\}) \\ u(t) = C_c x_c(t) + D_{1c} z_c(t) + D_{2c} F(C_p x_p(t) + D_p \Lambda\{u(t) + K_0[t, x_p(t)]\}) \end{cases} \tag{3}$$

Consequently, the second equation in Eq. (3) can be solved explicitly for $u(t)$:

$$\begin{aligned} u(t) &= (\mathbb{I} - D_{2c} F D_p \Lambda)^{-1}\{C_c x_c(t) + D_{1c} z_c(t) \\ &\quad + D_{2_c} F C_p x_p(t) + D_{2c} F D_p \Lambda K_0[t, x_p(t)]\} \\ &= (\mathbb{I} - D_{2c} F D_p \Lambda)^{-1}[D_{2c} F C_p \quad C_c] \underbrace{\begin{bmatrix} x_p(t) \\ x_c(t) \end{bmatrix}}_{x(t)} \\ &\quad + (\mathbb{I} - D_{2c} F D_p \Lambda)^{-1} D_{1c} z_c(t) \\ &\quad + (\mathbb{I} - D_{2c} F D_p \Lambda)^{-1} D_{2c} F D_p \Lambda K_0[t, x_p(t)] \end{aligned} \tag{4}$$

Assuming no uncertainties {i.e., $\Lambda = \mathbb{I}$, $K_0[t, x_p(t)] = \mathbf{0}$}, the baseline controller $u_L(t)$, can be written as

$$u_L(t) = K_x^\top x(t) + K_z^\top z_c(t) \tag{5}$$

where

$$\begin{aligned} K_x^\top &= (\mathbb{I} - D_{2c} F D_p)^{-1}[D_{2c} F C_p \quad C_c], \\ K_z^\top &= (\mathbb{I} - D_{2c} F D_p)^{-1} D_{1c} \end{aligned}$$

The extended system dynamics are

$$\begin{aligned} \underbrace{\begin{bmatrix} \dot{x}_p(t) \\ \dot{x}_c(t) \end{bmatrix}}_{\dot{x}(t)} &= \underbrace{\begin{bmatrix} A_p & 0 \\ B_{2c} F C_p & A_c \end{bmatrix}}_{A} \underbrace{\begin{bmatrix} x_p(t) \\ x_c(t) \end{bmatrix}}_{x(t)} + \underbrace{\begin{bmatrix} B_p \\ B_{2c} F D_p \end{bmatrix}}_{B_1} \Lambda\{u(t) \\ &\quad + K_0[t, x_p(t)]\} + \underbrace{\begin{bmatrix} 0 \\ B_{1c} \end{bmatrix}}_{B_2} z_c(t) \\ y(t) &= \underbrace{\{C_p \quad [0]\}}_{C} x(t) + D_p \Lambda\{u(t) + K_0[t, x_p(t)]\} \end{aligned} \tag{6}$$

or equivalently,

$$\begin{aligned} \dot{x}(t) &= Ax(t) + B_1 \Lambda\{u(t) + K_0[t, x_p(t)]\} + B_2 z_c(t) \\ y(t) &= Cx(t) + D_p \Lambda\{u(t) + K_0[t, x_p(t)]\} \end{aligned} \tag{7}$$

where $x \in \mathbb{R}^n$, $n = n_1 + n_2$.

In the absence of uncertainties, the linear closed-loop dynamics take the form:

$$\begin{aligned} \dot{x}_m(t) &= \underbrace{(A + B_1 K_x^\top)}_{A_m} x_m(t) + \underbrace{(B_1 K_z^\top + B_2)}_{B_m} z_c(t) \\ y_m(t) &= \underbrace{(C + D_p K_x^\top)}_{C_m} x_m(t) + \underbrace{D_p K_z^\top}_{D_m} z_c(t) \end{aligned} \tag{8}$$

The closed-loop system in Eq. (8) defines the desired nominal response, with A_m being Hurwitz. The control design relies on the following assumptions.

Assumption 1:

$$\Lambda_i \in [\Lambda_l, \quad \Lambda_u], \qquad i = 1, 2, \cdots, m \tag{9}$$

where $\Lambda_u > \Lambda_l > 0$ are known.

Let $f[t, x(t)] = \Lambda K_0[t, x_p(t)]$, where $f: \mathbb{R} \times \mathbb{R}^n \to \mathbb{R}^m$ is an unknown nonlinear function. Notice that

$$\|x_p\|_\infty \le \|x\|_\infty, \qquad \|x_{p1} - x_{p2}\|_\infty \le \|x_1 - x_2\|_\infty$$

Assumption 2 (semiglobal Lipschitz condition): For any $\delta > 0$, there exist positive L_δ and B, such that

$$\|f(t, x_1) - f(t, x_2)\|_\infty \le L_\delta \|x_1 - x_2\|_\infty \tag{10}$$

$$\|f(t, 0)\|_\infty \le B \tag{11}$$

for all $\|x_1\|_\infty \le \delta$ and $\|x_2\|_\infty \le \delta$ uniformly in $t \ge 0$.

Assumption 3 (semiglobal uniform boundedness of partial derivatives): For any $\delta > 0$, there exist $\mathrm{d}_{f_x}(\delta) > 0$ and $\mathrm{d}_{f_t}(\delta) > 0$,

such that for any $\|x\|_\infty \le \delta$, the partial derivatives of $f(t, x)$ are piecewise continuous and bounded:

$$\left\|\frac{\partial f(t, x)}{\partial x}\right\|_\infty \le \mathrm{d}_{f_x}(\delta), \qquad \left\|\frac{\partial f(t, x)}{\partial t}\right\|_\infty \le \mathrm{d}_{f_t}(\delta) \tag{12}$$

The control objective is to design state feedback control $u(t)$, such that the system state $x(t)$ tracks the desired model state $x_m(t)$ in the presence of system uncertainties Λ and $K_0[t, x_p(t)]$ with quantifiable transient performance. Next, we present the $\mathcal{L}_1$ adaptive controller that achieves this objective without the need for any retuning.

III. $\mathcal{L}_1$ Adaptive Control

A. Introduction to $\mathcal{L}_1$ Adaptive Control

The $\mathcal{L}_1$ adaptive controller, as compared with the alternative solutions in adaptive control, attempts to compensate only for the portion of uncertainties that are within the control channel bandwidth. This is reflected in its problem formulation and the definition of the nominal controller associated with the reference system. Because this reference system depends upon uncertainties, its stability depends upon the bandwidth of the low-pass filter. A small-gain-theorem-type argument relates the bandwidth of this filter to the growth rate of the nonlinearities, referred to as the Lipschitz constant in the sequel. Thus, as compared with standard model reference adaptive control (MRAC) algorithms, the $\mathcal{L}_1$ adaptive controller is less ambitious in terms of its reference system, but it gives the opportunity to decouple adaptation from robustness, as the low-pass filter in the feedback path gives the opportunity to ensure uniform performance bounds for system input and output signals in the presence of fast adaptation. Thus, the low-pass filter gives the opportunity to appropriately band the frequencies in the control signal, and it ensures that both signals of the closed-loop system (state and input) follow the same signals of the closed-loop bounded reference system (both in the transient and steady state). The remaining question is the performance of this reference system in the presence of uncertainties. It is straightforward to notice that increasing the bandwidth of the filter implies that the signals of this closed-loop reference system approximate the signals of the ideal desired reference system, typically used in MRAC-type feedback architectures, albeit at the price of a reduced time-delay margin. Thus, by appropriately modifying the control objective, the $\mathcal{L}_1$ adaptive controller shifts the tuning of the performance/robustness of a closed-loop adaptive architecture from the selection of the (adaptation) rate of the nonlinear gradient minimization scheme (governing the adaptive law) to the selection of the bandwidth of a low-pass filter, which can be systematically addressed using tools from the classical and robust control. The latter problem is linear in its nature and can be resorted to linear matrix inequality (LMI)-type conditions [16].

B. Controller Structure

Consider the following control law:

$$u(t) = u_L(t) + u_{\mathrm{ad}}(t) \tag{13}$$

where $u_L(t)$ is the component of the baseline linear controller, and $u_{\mathrm{ad}}(t)$ is the adaptive increment. The baseline controller is defined in Eq. (5), which is repeated here:

$$u_L(t) = K_x^\top x(t) + K_z^\top z_c(t) \tag{14}$$

where K_x and K_z denote the $(n \times m)$ and $(q \times m)$ nominal feedback and feedforward gain matrices, correspondingly. The system dynamics in Eq. (6) take the form:

$$\begin{aligned}\dot{x}(t) &= (A + B_1\Lambda K_x^T)x(t) + B_1\Lambda\{u_{\mathrm{ad}} + K_0[t, x_p(t)]\} \\ &\quad + (B_2 + B_1\Lambda K_z^T)z_c(t)\end{aligned} \tag{15}$$

From Eqs. (8) and (15), we have

$$\begin{aligned}\dot{x}(t) &= A_m x(t) + B_m z_c(t) + B_1\{\Lambda u_{\mathrm{ad}}(t) + \Lambda K_0[t, x_p(t)] \\ &\quad + k_x^\top x(t) + k_z^\top z_c(t)\}\end{aligned} \tag{16}$$

where

$$k_x^\top = (\Lambda - I)K_x^\top, \qquad k_z^\top = (\Lambda - I)K_z^\top \tag{17}$$

Remark 1: In the absence of actuator failures (i.e., when $\Lambda = I_m$), we have $k_x(t) = 0_{n\times m}$ and $k_z(t) = 0_{q\times m}$. This implies that the adaptive system augments the baseline inner-loop controller, and therefore the incremental adaptive feedback gains can be initialized at zero.

The design of the $\mathcal{L}_1$ adaptive controller involves a diagonal transfer function matrix $D(s)$ with strictly proper transfer function elements and a positive diagonal feedback gain matrix $k \in \mathbb{R}^{m\times m}$:

$$D(s) = \begin{bmatrix} D_1(s) & 0 & 0 & \cdots & 0 \\ 0 & D_2(s) & 0 & \cdots & 0 \\ 0 & 0 & \ddots & \cdots & 0 \\ \vdots & \vdots & \vdots & \ddots & \vdots \\ 0 & 0 & 0 & \cdots & D_m(s) \end{bmatrix} \tag{18}$$

$$k = \begin{bmatrix} k_1 & 0 & 0 & \cdots & 0 \\ 0 & k_2 & 0 & \cdots & 0 \\ 0 & 0 & \ddots & \cdots & 0 \\ \vdots & \vdots & \vdots & \ddots & \vdots \\ 0 & 0 & 0 & \cdots & k_m \end{bmatrix} \tag{19}$$

which leads to strictly proper and stable

$$C(s) = \begin{bmatrix} C_1(s) & 0 & 0 & \cdots & 0 \\ 0 & C_2(s) & 0 & \cdots & 0 \\ 0 & 0 & \ddots & \cdots & 0 \\ \vdots & \vdots & \vdots & \ddots & \vdots \\ 0 & 0 & 0 & \cdots & C_m(s) \end{bmatrix}$$

$$C_i(s) = \frac{\Lambda_i k_i D_i(s)}{1 + \Lambda_i k_i D(s)}, \qquad i = 1, 2, \cdots, m \tag{20}$$

with low-pass gain $C_i(0) = 1$. One simple choice is

$$D_i(s) = \frac{1}{s} \tag{21}$$

which yields a first-order strictly proper $C(s)$ in the following form:

$$C(s) = \begin{bmatrix} \frac{\Lambda_1 k_1}{s+\Lambda_1 k_1} & 0 & 0 & \cdots & 0 \\ 0 & \frac{\Lambda_2 k_2}{s+\Lambda_2 k_2} & 0 & \cdots & 0 \\ 0 & 0 & \ddots & \cdots & 0 \\ \vdots & \vdots & \vdots & \cdots & \vdots \\ 0 & 0 & 0 & \cdots & \frac{\Lambda_m k_m}{s+\Lambda_m k_m} \end{bmatrix} \tag{22}$$

Further, let

$$\begin{aligned}L_x &= \max\{|\Lambda_l - 1|, |\Lambda_u - 1|\}\|K_x^\top\|_{\mathcal{L}_1} = \max\{|\Lambda_l - 1|, |\Lambda_u \\ &\quad - 1|\}\max_{i=1,2,\cdots,m}\left(\sum_{j=1}^{n}|K_{x_{ji}}|\right) \\ L_z &= \max\{|\Lambda_l - 1|, |\Lambda_u - 1|\}\|K_z^\top\|_{\mathcal{L}_1} = \max\{|\Lambda_l - 1|, |\Lambda_u \\ &\quad - 1|\}\max_{i=1,2,\cdots,m}\left(\sum_{j=1}^{n}|K_{z_{ji}}|\right)\end{aligned} \tag{23}$$

where $K_{x_{ji}}(t)$ are the jth row ith column element of K_x. We now state the $\mathcal{L}_1$ performance requirement that ensures stability of the entire system and desired transient performance, as in [11].

Let

$$H(s) = (s\mathbb{I} - A_m)^{-1}B_1 \tag{24}$$

$$H_m(s) = (s\mathbb{I} - A_m)^{-1}B_m \tag{25}$$

and $r_0(t)$ be the signal with its Laplace transformation $(s\mathbb{I} - A_m)^{-1}x_0$. Because A_m is Hurwitz and x_0 is finite, $\|r_0\|_{\mathcal{L}_\infty}$ is finite.

For the $\mathcal{L}_1$-norm upper bound, the choice of $D(s)$ and k needs to ensure that there exists ρ_r, such that

$$\|G(s)\|_{\mathcal{L}_1} < (\rho_r - (\|G(s)\|_{\mathcal{L}_1}L_z + \|H_m(s)\|_{\mathcal{L}_1})\|z_c\|_{\mathcal{L}_\infty} - \|r_0\|_{\mathcal{L}_\infty})/(\rho_r L_{\rho_r} + \rho_r L_x + B) \tag{26}$$

where

$$G(s) = H(s)[\mathbb{I}_{m\times m} - C(s)]$$

and L_{ρ_r} is defined in Eq. (10) with substitution of δ by ρ_r.

Remark 2: We notice that the $\mathcal{L}_1$-norm upper bound in Eq. (26) is a consequence of the semiglobal Lipschitz property of $f(t, x)$, stated in Assumption 1. If $f(t, x)$ is globally Lipschitz with a uniform Lipschitz constant L_g, then

$$\lim_{\rho_r\to\infty}(\rho_r - (\|G(s)\|_{\mathcal{L}_1}L_z + \|H_m(s)\|_{\mathcal{L}_1})\|z_c\|_{\mathcal{L}_\infty} - \|r_0\|_{\mathcal{L}_\infty})/(\rho_r L_g + \rho_r L_x + B) = \frac{1}{L_g + L_x} = \frac{1}{L}$$

where $L = L_g + L_x$, and the $\mathcal{L}_1$-norm upper bound in Eq. (26) degenerates into

$$\|G(s)\|_{\mathcal{L}_1} < 1/L$$

which is the same as the one derived in [9] for systems with constant unknown parameters. Notice that Eq. (26) is a sufficient condition for stability.

The elements of the $\mathcal{L}_1$ adaptive controller are introduced next. We consider the following state predictor:

$$\begin{aligned}\dot{\hat{x}}(t) &= A_m\hat{x}(t) + B_m z_c(t) + B_1[\hat{\Lambda}(t)u_{\text{ad}}(t) + \hat{\theta}^\top(t)\|x(t)\|_\infty \\ &\quad + \hat{\sigma}^\top(t) + \hat{k}_x^\top(t)x(t) + \hat{k}_z^\top(t)z_c(t)] \\ \hat{y}(t) &= c^\top\hat{x}(t), \qquad \hat{x}(0) = x_0\end{aligned} \tag{27}$$

where $\hat{\theta}(t) \in \mathbb{R}^{1\times m}$ and $\hat{\sigma}(t) \in \mathbb{R}^{1\times m}$.

The adaptive estimates $\hat{\Lambda}(t)$, $\hat{\theta}(t)$, $\hat{\sigma}(t)$, $\hat{k}_x(t)$, and $\hat{k}_z(t)$ are governed by the following adaptation laws:

$$\begin{aligned}\dot{\hat{\theta}}(t) &= \Gamma_\theta\,\text{Proj}[\hat{\theta}(t), -\|x(t)\|_\infty\tilde{x}^\top(t)PB_1], \qquad \hat{\theta}(0) = \hat{\theta}_0 \\ \dot{\hat{\sigma}}(t) &= \Gamma_\sigma\,\text{Proj}[\hat{\sigma}(t), -\tilde{x}^\top(t)PB_1], \qquad \hat{\sigma}(0) = \hat{\sigma}_0 \\ \dot{\hat{\Lambda}}(t) &= \Gamma_\Lambda\,\text{Proj}[\hat{\Lambda}(t), -u_{\text{ad}}(t)\tilde{x}^\top(t)PB_1], \qquad \hat{\Lambda}(0) = \hat{\Lambda}_0 \\ \dot{\hat{k}}_x(t) &= \Gamma_{kx}\,\text{Proj}[\hat{k}_x(t), -x(t)\tilde{x}^\top(t)PB_1], \qquad \hat{k}_x(0) = 0 \\ \dot{\hat{k}}_z(t) &= \Gamma_{kz}\,\text{Proj}[\hat{k}_z(t), -z_c(t)\tilde{x}^\top(t)PB_1], \qquad \hat{k}_z(0) = 0\end{aligned}$$

where $\tilde{x}(t) = \hat{x}(t) - x(t)$, $\Gamma_\theta = \Gamma\mathbb{I}_{1\times 1}$, $\Gamma_\sigma = \Gamma\mathbb{I}_{1\times 1}$, $\Gamma_\Lambda = \Gamma\mathbb{I}_{m\times m}$, $\Gamma_{kx} = \Gamma\mathbb{I}_{n\times n}$, and $\Gamma_{kz} = \Gamma\mathbb{I}_{q\times q}$ are the adaptation gain matrices, P is the solution of the algebraic equation $A_m^\top P + PA_m = -Q$, $Q > 0$, and the projection operator ensures that the adaptive estimates $\hat{\Lambda}(t)$, $\hat{\theta}(t)$, $\hat{\sigma}(t)$, $\hat{k}_x(t)$, and $\hat{k}_z(t)$ remain inside the compact sets $[\omega_l, \omega_u]$, $[-\theta_b, \theta_b]$, $[-\sigma_b, \sigma_b]$, $[-L_x, L_x]$, and $[-L_z, L_z]$, respectively, with θ_b and σ_b defined as follows:

$$\theta_b = L_\rho, \qquad \sigma_b = B + \epsilon \tag{28}$$

where ϵ is an arbitrary positive constant and

$$\rho = \rho_r + \beta \tag{29}$$

with β being an arbitrary positive constant as well. The constant L_ρ is defined in Eq. (10) with the substitution of δ by ρ.

For the control law, the control signal is generated through the feedback loop of the following system:

$$\chi(s) = D(s)\bar{r}(s), \qquad u_{\text{ad}}(s) = -k\chi(s) \tag{30}$$

where $\bar{r}(s)$ is the Laplace transformation of

$$\bar{r}(t) = \hat{\Lambda}(t)u_{\text{ad}}(t) + \hat{\theta}^\top(t)\|x(t)\|_\infty + \hat{\sigma}^\top(t) + \hat{k}_x^\top(t)x(t) + \hat{k}_z^\top(t)z_c(t) \tag{31}$$

The complete $\mathcal{L}_1$ adaptive controller consists of Eqs. (27), (28), and (30) subject to the $\mathcal{L}_1$-norm upper bound in Eq. (26).

IV. Analysis of $\mathcal{L}_1$ Adaptive Controller

A. Reference System

We now consider the following closed-loop reference system, with its control signal and system response being defined as follows:

$$\dot{x}_{\text{ref}}(t) = A_m x_{\text{ref}}(t) + B_m z_c(t) + B_1\{f[t, x_{\text{ref}}(t)] + \Lambda u_{\text{ref}}(t) + k_x^\top x_{\text{ref}} + k_z^\top z_c(t)\} \tag{32}$$

$$u_{\text{ref}}(s) = -\Lambda^{-1}C(s)\bar{r}_{\text{ref}}(s) \tag{33}$$

$$y_{\text{ref}}(t) = c^\top x_{\text{ref}}(t), \qquad x_{\text{ref}}(0) = x_0 \tag{34}$$

where $\bar{r}_{\text{ref}}(s)$ is the Laplace transformation of the signal $\bar{r}_{\text{ref}}(t) = f[t, x_{\text{ref}}(t)] + k_x^\top x_{\text{ref}}(t) + k_z^\top z_c(t)$. The next Lemma establishes the stability of the closed-loop system in Eqs. (32–34).

Lemma 1: For the closed-loop reference system in Eqs. (32–34), subject to the $\mathcal{L}_1$-norm stability condition in Eq. (26), we have

$$\|x_{\text{ref}}\|_{\mathcal{L}_\infty} < \rho_r \tag{35}$$

$$\|u_{\text{ref}}\|_{\mathcal{L}_\infty} < \rho_{u_r} \tag{36}$$

where ρ_r is defined in Eq. (26), and

$$\rho_{u_r} = \|\Lambda^{-1}C(s)\|_{\mathcal{L}_1}(L_{\rho_r}\rho_r + L_x\rho_r + B + L_z\|z_c\|_{\mathcal{L}_\infty})$$

A proof can be found in [11].

B. Equivalent Linear Time-Varying System

In this section, we demonstrate that the nonlinear system in Eq. (16) can be transformed into a linear system with unknown time-varying parameters. We need to first introduce several notations. Choose γ_0 to satisfy

$$\gamma_1 \triangleq \frac{\|C(s)\|_{\mathcal{L}_1}}{1 - \|G(s)\|_{\mathcal{L}_1}L_\rho}\gamma_0 + \beta_1 < \beta \tag{37}$$

where $0 < \beta_1 < \beta$ is an arbitrary positive constant. We notice that γ_0 can be arbitrarily small, because β and β_1 can be set arbitrarily. We will prove that by increasing the adaptive gain, γ_0 can serve as an upper bound for the error signal $\tilde{x}(t)$. Define

$$\begin{aligned}B_r &\triangleq [B_1\bar{B}_1], \qquad H_r(s) \triangleq (sI - A_m)^{-1}B_r \\ C_r(s) &\triangleq \begin{bmatrix}\Lambda^{-1}C(s) & 0 \\ 0 & \bar{C}(s)\end{bmatrix}\end{aligned} \tag{38}$$

where the choice of $\bar{B}_1$ renders $B_r \in \mathbb{R}^{n\times n}$ full rank, and $\bar{C}(s)$ is an arbitrary diagonal strictly proper stable transfer function that yields a $C_r(s) \in \mathbb{R}^{n\times n}$ of appropriate dimension. Further, let

$$\rho_u = \rho_{u_r} + \gamma_2 \tag{39}$$

$$\gamma_2 = \|\Lambda^{-1}C(s)\|_{\mathcal{L}_1}(L_\rho + L_x)\gamma_1 + \|\Lambda^{-1}C_rH_r^{-1}\|_{\mathcal{L}_1}\gamma_0 \tag{40}$$

Lemma 2: If

$$\|x_t\|_{\mathcal{L}_\infty} \le \rho \tag{41}$$

$$\|u_t\|_{\mathcal{L}_\infty} \le \rho_u \tag{42}$$

where $\|(\cdot)_t\|_{\mathcal{L}_\infty}$ denotes the truncated $\mathcal{L}_\infty$ norm (see Appendix for definition), there exist differentiable $\theta(\tau)$ and $\sigma(\tau)$ with bounded $\dot{\theta}(\tau)$ and $\dot{\sigma}(t)$ over $\tau \in [0, t]$, such that

$$\|\theta(\tau)\|_\infty < \theta_b \tag{43}$$

$$\|\sigma(\tau)\|_\infty < \sigma_b \tag{44}$$

$$f[\tau,\ x(\tau)] = \theta(\tau)\|x(\tau)\|_\infty + \sigma(\tau) \tag{45}$$

Refer to [11] for the proof.
Because

$$\|x_0\|_\infty \le \rho_r \le \rho, \qquad u(0) = 0 \tag{46}$$

and $x(t)$ and $u(t)$ are continuous, there always exists t, such that

$$\|x_t\|_{\mathcal{L}_\infty} \le \rho, \qquad \|u_t\|_{\mathcal{L}_\infty} \le \rho_u \tag{47}$$

It follows from Eq. (47) and Lemma 2 that the system in Eq. (16) can be rewritten over $[0,\ t]$ as

$$\begin{aligned}\dot{x}(\tau) &= A_m x(\tau) + B_m z_c(\tau) + B_1(\theta^\top(\tau)\|x(\tau)\|_\infty + \Lambda u_{\text{ad}}(\tau)\\ &\quad + \sigma(\tau) + k_x^\top x(\tau) + k_z^\top z_c(\tau))\\ y(\tau) &= c^\top x(\tau), \qquad x(0) = x_0\end{aligned} \tag{48}$$

where $\theta(\tau)$ and $\sigma(\tau)$ are unknown time-varying signals subject to

$$|\theta(\tau)| < \theta_b, \qquad |\sigma(\tau)| < \sigma_b, \quad \forall\ \tau \in [0, t] \tag{49}$$

$$|\dot{\theta}(\tau)| \le d_\theta(\rho, \rho_u), \qquad |\dot{\sigma}(\tau)| \le d_\sigma(\rho, \rho_u), \quad \forall\ \tau \in [0, t]. \tag{50}$$

C. Transient and Steady-State Performance

Theorem 1: Consider the reference system in Eqs. (32–34) and the closed-loop $\mathcal{L}_1$ adaptive controller in Eqs. (16), (27), (28), and (30) subject to Eq. (26). If the adaptive gain is chosen to verify the lower bound,

$$\Gamma > \frac{\theta_m(\rho,\ \rho_u)}{\lambda_{\min}(P)\gamma_0^2} \tag{51}$$

where

$$\begin{aligned}\theta_m(\rho,\ \rho_u) &\triangleq 4m^2\theta_b^2 + 4m^2\sigma_b^2 + m^2(\Lambda_u - \Lambda_l)^2 + 4m^2L_x^2\\ &\quad + 4m^2L_z^2 + 4\frac{\lambda_{\max}(P)}{\lambda_{\min}(Q)}[\theta_b d_\theta(\rho,\ \rho_u) + \sigma_b d_\sigma(\rho,\ \rho_u)]\end{aligned} \tag{52}$$

we have

$$\|\tilde{x}\|_{\mathcal{L}_\infty} \le \gamma_0 \tag{53}$$

$$\|x - x_{\text{ref}}\|_{\mathcal{L}_\infty} < \gamma_1 \tag{54}$$

$$\|u - u_{\text{ref}}\|_{\mathcal{L}_\infty} < \gamma_2 \tag{55}$$

where γ_1 and γ_2 are defined in Eqs. (37) and (40).

See [11] for proof details. It follows from Eq. (51) that we can achieve arbitrarily small γ_0 by increasing the adaptive gain.

D. Time-Delay Margin

In this case, when the nonlinearity permits the following representation:

$$f[t,\ x(t)] = \theta^\top x(t) + \sigma(t)$$

where θ is a constant vector, the time-delay margin of the $\mathcal{L}_1$ adaptive controller can be computed analytically [10]. The dynamics in Eq. (16) can be rewritten as

$$\begin{aligned}\dot{x}(t) &= A_m x(t) + B_m z_c(t) + B_1[\Lambda u_{\text{ad}}(t) + \theta^\top x(t) + k_x^\top x(t)\\ &\quad + \sigma(t) + k_z^\top z_c(t)]\end{aligned} \tag{56}$$

Define

$$\bar{H}(s) = (s\mathbb{I} - A_m - B_1\theta^\top - B_1k_x^\top)^{-1}B_1$$

Following the results in [10], when $\Gamma \to \infty$, the time-delay margin of the closed-loop $\mathcal{L}_1$ adaptive control system has a conservative lower bound, which is given by the time-delay margin of the following open-loop LTI system:

$$H_o(s) = \frac{C(s)}{1 - C(s)}[1 + (\theta^\top + k_x^\top)\bar{H}(s)] \tag{57}$$

Because, in this structure, $C(s)$ is decoupled from $\bar{H}(s)$, it is obvious that one can choose $C(s)$ judiciously to maximize the phase margin of the open-loop transfer function $H_o(s)$ and minimize its crossover frequency to obtain a larger time-delay margin. Although analytical derivation of the time-delay margin for multi-input–multi-output systems with more general unknown nonlinear function $f[t,\ x(t)]$ is not available,[§] we use insights from this analysis for the selection of $C(s)$ to tune the time-delay margin in the applications discussed next.

E. Design Guidelines

We note that the control law $u_{\text{ref}}(t)$ in the closed-loop reference system, which is used in the analysis of $\mathcal{L}_\infty$-norm bounds, is not implementable because its definition involves the unknown parameters. Theorem 1 ensures that the $\mathcal{L}_1$ adaptive controller approximates $u_{\text{ref}}(t)$ both in transient and steady state. And so, it is important to understand how these bounds can be used for ensuring uniform transient response with desired specifications. We notice that the following ideal control signal

$$u_{\text{id}}(t) = \Lambda^{-1}\{-f[t, x_{\text{id}}(t)] + k_x^\top x_{\text{id}}(t) + k_z^\top z_c(t)\} \tag{58}$$

is the one that leads to the desired system response:

$$\dot{x}_{\text{id}}(t) = A_m x_{\text{id}}(t) + B_m z_c(t), \qquad y_{\text{id}}(t) = c^\top x_{\text{id}}(t) \tag{59}$$

by canceling the uncertainties exactly. In the closed-loop reference system in Eqs. (32–34), $u_{\text{id}}(t)$ is further low-pass filtered by $C(s)$ to have guaranteed low-frequency range. Thus, the reference system in Eqs. (32–34) has a different response as compared with Eq. (59), achieved with Eq. (58). We refer the reader to [13] for specific design guidelines on the selection of $C(s)$ to ensure that the response of $x_{\text{ref}}(t)$ and $u_{\text{ref}}(t)$ can be made as close as possible to Eq. (59).

We notice that the tradeoff between the time-delay margin and the performance of the $\mathcal{L}_1$ adaptive controller depends solely upon the bandwidth of $C(s)$. Increasing the bandwidth of $C(s)$ leads to improved performance at the price of a reduced time-delay margin. In [16], we consider constrained optimization of the performance and/or the robustness of the $\mathcal{L}_1$ adaptive controller by resorting to appropriate LMI-type conditions. If the corresponding LMI has a

[§]The fact that this analytical derivation is somewhat complicated follows from the fact that, for open-loop nonlinear systems, there are no general results for computing the time-delay margin (as one has for linear systems) expressed via the phase margin and the crossover frequency.

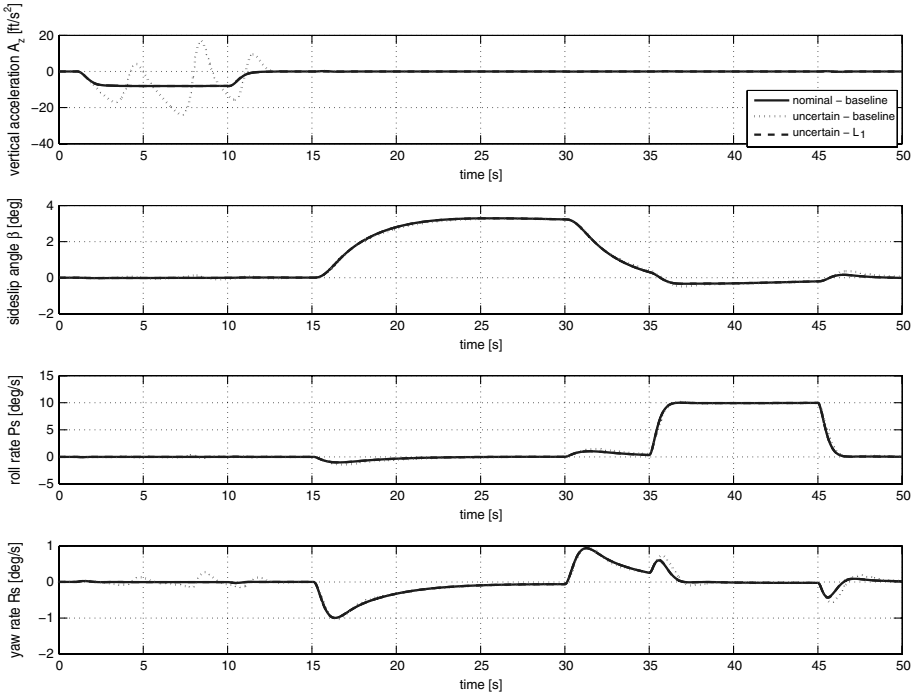

Fig. 1 Inner-loop adaptation with control effectiveness reduction and pitch break phenomenon (command tracking).

solution, then the desired performance bound can be achieved while retaining a prespecified lower bound on the time-delay margin.

V. Unmanned Combat Aerial Vehicle

The $\mathcal{L}_1$ adaptive controller is applied to a model of the aerodynamically unstable X-45A UCAV in the presence of control effectiveness reduction and pitch break uncertainty [unknown nonlinear in angle of attack (AOA) pitching moment increment]. This uncertainty is introduced in pitch dynamics in order to model unknown changes in the aircraft pitching moment that can drive the aircraft into an uncontrollable (in AOA) region.

We recall the aircraft dynamics from Eq. (7):

$$\dot{x}(t) = Ax(t) + B_1\Lambda\{u(t) + K_0[t,\, x_p(t)]\} + B_2 z_c(t)$$
$$x(0) = x_0 = 0 \tag{60}$$

where $x(t) \in \mathbb{R}^9$, $u(t) \in \mathbb{R}^3$ (virtual control input), and $z_c(t) \in \mathbb{R}^4$ are the measured system states, control signals, and reference inputs, respectively, and $A \in \mathbb{R}^{9\times 9}$, $B_2 \in \mathbb{R}^{9\times 4}$, and $B_1 \in \mathbb{R}^{9\times 3}$ are known matrices, from which the three columns of B_1 are linearly independent:

$$\Lambda = \begin{bmatrix} \Lambda_1 & 0 & 0 \\ 0 & \Lambda_2 & 0 \\ 0 & 0 & \Lambda_3 \end{bmatrix} \tag{61}$$

is an unknown diagonal matrix with strictly positive diagonal elements. The state vector $x = (\alpha,\, \beta,\, p,\, q,\, r,\, q_I,\, p_I,\, r_I,\, r_w)^\top$ comprises five plant states x_p, which include the AOA α, the angle of side slip β, the body roll rate p, the body pitch rate q, the body yaw rate r, and the four baseline controller x_c states, which include pitch, roll, and yaw (q_I, p_I, and r_I) integrator states and the yaw rate

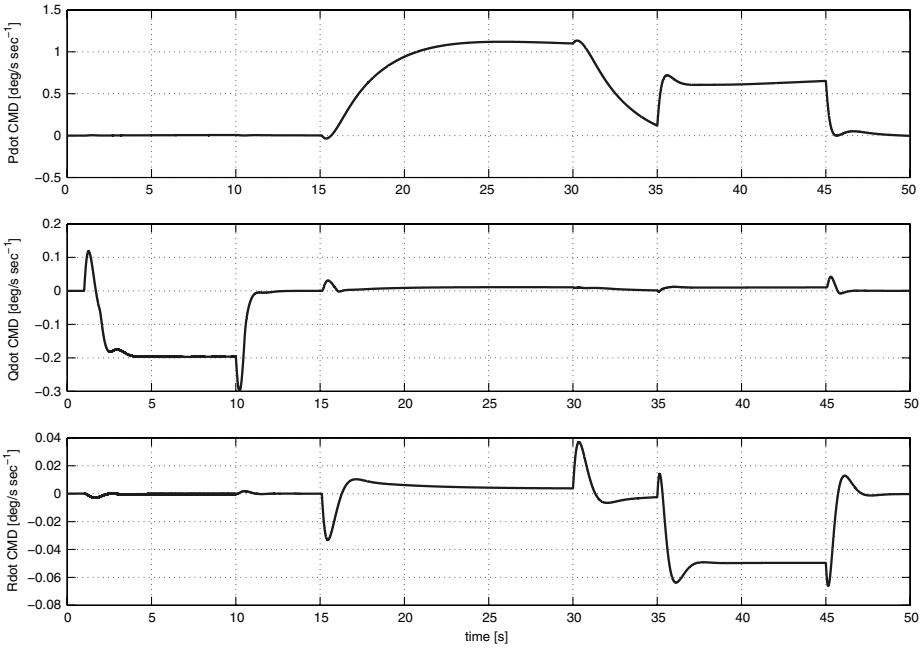

Fig. 2 Inner-loop adaptation with control effectiveness reduction and pitch break phenomenon (virtual controls).

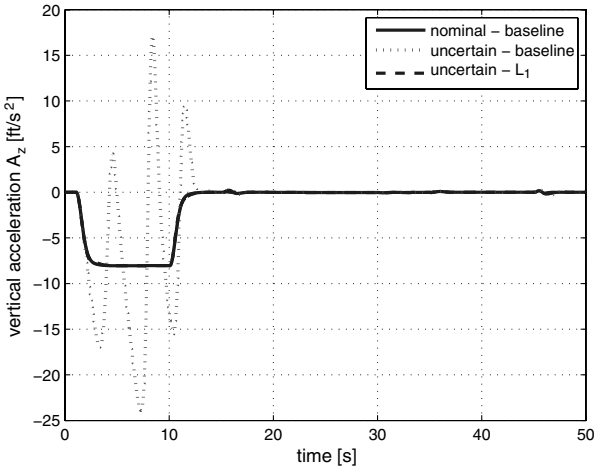

Fig. 3 Zoomed subplot of Fig. 2 to show guaranteed $\mathcal{L}_1$ performance.

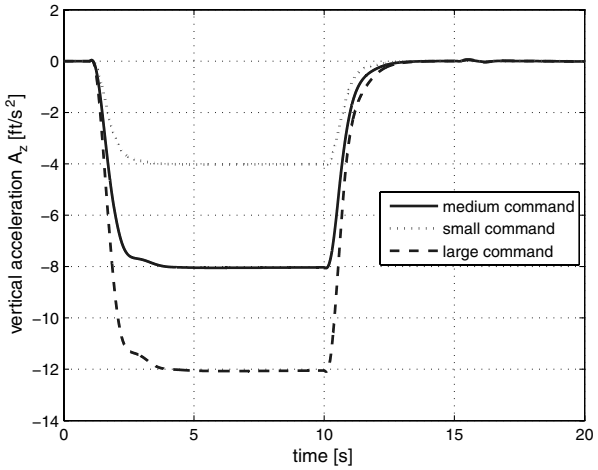

Fig. 4 Inner-loop adaptation with control effectiveness reduction and pitch break phenomenon (scaled command tracking).

washout filter signal r_w. The vector $z_c = (A_z^{\text{cmd}},\ \beta^{\text{cmd}},\ p^{\text{cmd}},\ r^{\text{cmd}})^\top$ consists of four inner-loop commands that include vertical acceleration, side slip, roll rate, and yaw rate, whereas $u(t)$ is the vector of virtual controls (roll, pitch, and yaw controls). Considering the control signal $u(t) = u_L(t) + u_{\text{ad}}(t)$, where $u_L(t)$ is defined in Eq. (5), the partially closed-loop system from Eq. (16) is repeated here:

$$\dot{x}(t) = A_m x(t) + B_m z_c(t) + B_1\{\Lambda u_{\text{ad}}(t) + f[t,\ x(t)] + k_x^\top x(t) + k_z^\top z_c(t)\} \tag{62}$$

where the adaptive control signal $u_{\text{ad}}(t)$ is defined according to the $\mathcal{L}_1$ adaptive controller in Eqs. (27), (28), and (30), subject to the $\mathcal{L}_1$-norm upper bound in Eq. (26), and $f[t,\ x(t)] = \Lambda K_0[t,\ x_p(t)]$. This is different from the approach, presented in [17], for which the radial basis function (RBF) approximation was employed for approximation of the nonlinearity. This significantly reduces the design effort by eliminating the need for RBF distributions and center/width tuning.

Note that the vector function $f[t,\ x(t)]$ represents the matched unknown nonlinearities, and Λ models the loss of control effectiveness caused by actuator failure(s) or damage(s) or combinations of them. The matrix Λ is defined in a way that each diagonal element of Λ represents a scaling factor for control effectiveness in a particular input channel. Thus, Λ is diagonal and is different from the control allocation matrix, which has already been incorporated in B_1 in Eq. (60). When some of the control surfaces fail or are damaged, the scaling factor for each virtual control will change. In simulations described next, we assume that the failure/damage situations will not cause the change of sign in the diagonal elements of Λ. This may exclude certain types of actuator failures (for example, complete loss of controllability of some control surfaces). However, as shown in our simulations, control effectiveness reduction (even a small amount of reduction) can degrade the output performance significantly. The $\mathcal{L}_1$ adaptive controller is shown to recover the nominal performance in the presence of the uncertain control effectiveness, subject to Assumption 1.[¶]

The inner-loop control objective is to design a full-state feedback controller $u_{\text{ad}}(t)$ for Eq. (62), such that all closed-loop signals remain bounded, and the system state tracks the state of a desired reference model in the presence of uncertainties and control effectiveness reduction. We compare the performance of the nominal plant in the presence of pitch break and control effectiveness reduction with the performance of the closed-loop system with the $\mathcal{L}_1$ adaptive controller. For the $\mathcal{L}_1$ adaptive controller, we set $k_i = 20$, where $i = 1$, 2, and 3, and $D_i(s) = \frac{1}{s}$, which verifies the $\mathcal{L}_1$-norm upper bound, and we set $\Gamma = 100,000$. The results are shown in Figs. 1 and 2. In Fig. 2, Pdot CMD, Qdot CMD, and Rdot CMD represent the virtual control commands (roll, pitch, and yaw controls). For comparison purposes, simulation data are obtained from the following three closed-inner-loop systems: a) adaptation off, uncertainties off; b) adaptation off, uncertainties on; and c) $\mathcal{L}_1$ adaptation on, uncertainties on.

Figures 1 and 2 demonstrate the benefits of adaptation when the control effectiveness reduction of each control surface occurs at 1 s and the pitch break phenomenon is active throughout the entire maneuver. The reduction of up to 30% of the control effectiveness for each actuator channel changes the Λ matrix to the following:

$$\Lambda = \begin{bmatrix} 0.7 & 0 & 0 \\ 0 & 0.7 & 0 \\ 0 & 0 & 0.7 \end{bmatrix}$$

Figure 1 indicates that, in spite of the control effectiveness reduction and pitch break uncertainty, the $\mathcal{L}_1$ adaptive system is able to quickly reconfigure and track the commanded vertical acceleration, the side-slip angle, the roll rate, and the yaw rate signals simultaneously. In fact, Fig. 1 shows that, with the adaptation turned on, the desired/nominal system tracking behavior has been recovered. In addition, Fig. 2 compares the three virtual control feedback signals and confirms that the level of control activity is reasonable. In Fig. 3, the subplot of Fig. 1 is replotted to show the perfect tracking achieved by $\mathcal{L}_1$ for vertical acceleration.

When the reference commands change, the system output and input have scaled responses similar to those of linear systems. These are shown in Figs. 4 and 5. Notice that the scaled responses are achieved in the absence of any saturation constraints.[**]

Next, we discuss the robustness of the scheme. The time-delay margin for the inner loop (without adaptive feedback) can be computed from the phase margin of the open-loop transfer functions. The open-loop transfer functions are calculated by breaking the virtual control ($\dot{p}$, $\dot{q}$, and $\dot{r}$) command loops one at a time, keeping the other two loops closed. This is shown in Table 1.

To calculate the time-delay margin for the adaptive system, we introduce the time delay at the plant input and compute the margins using numerical simulations.

The time-delay margins for the $\mathcal{L}_1$ adaptive scheme are summarized in Table 2 for $C(s) = 1/(0.05s + 1)$ and $\Gamma = 100,000$. The zoomed vertical acceleration response in the presence of a certain amount of time delay (e.g., 0.05 s for each control channel) is shown in Fig. 6. The worst-case time-delay margin is 0.062 s. Following the discussion from Sec. IV.D, we can improve

[¶]We note that in [17], a broader class of uncertainties has been considered that violates Assumption 1, and the performance of the $\mathcal{L}_1$ adaptive controller has been verified for that class of uncertainties as well.

[**]The $\mathcal{L}_1$ adaptive controller in the presence of saturation is considered in [18]. The uniform performance bounds, with respect to a reference system, which also accounts for saturation explicitly, are shown to be inverse proportional to the rate of adaptation.

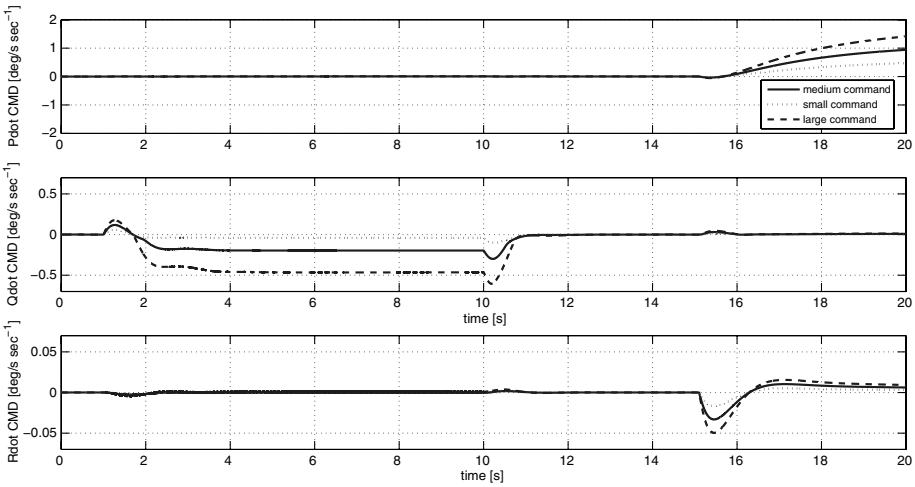

Fig. 5 Inner-loop adaptation with control effectiveness reduction and pitch break phenomenon: scaled virtual control.

the time-delay margin by tuning $C(s)$. Toward that end, consider the following low-pass filter:

$$C_1(s) = \frac{1}{0.05s+1}\frac{(-6s+1)^2}{(8s+1)^2}$$

for which the $\mathcal{L}_1$-norm upper bound holds. The corresponding $D_1(s)$ will be

$$D_1(s) = \frac{(-6s+1)^2}{s(3.2s^2+28.8s+28.05)}$$

The Bode plots of $D(s)$ and $D_1(s)$ are given in Fig. 7. Note that a nonminimum phase filter is used to enhance the phase characteristic in the region of the frequency band in order to improve the phase margin.

The subplot of vertical acceleration of Fig. 1 is repeated with $C_1(s)$ in Fig. 8. We see that there is some degradation in the tracking; however, it is still satisfactory. For this choice of $C_1(s)$, the worst-case time-delay obtained from simulation is 0.15 s. In Table 2, we have the worst-case time-delay margin for $C(s)$ equal to 0.062 s, which implies that $C_1(s)$ doubles the time-delay margin. Thus, at this stage, it appears that improving the time-delay margin hurts the transient performance, which is consistent with the conventional claims in the linear systems theory. From this perspective, the $\mathcal{L}_1$ adaptive controller achieves clear separation between adaptation and robustness; the adaptation can be as fast as the CPU permits, although robustness/performance tradeoff is reduced to the filter design and can be addressed via conventional methods well known from classical and robust control. We note that all the time-delay margins are calculated for the case of control effectiveness reduction and in the presence of the pitch break uncertainty.

However, we note that a smaller value of Γ is preferable from an implementation point of view. Figure 9 shows the system response for different values of Γ for both low-pass filters. It can be seen that there is almost no degradation in the time response performance. However, for the low-pass filter $C(s) = 1/(0.05s+1)$, if we decrease Γ from 100,000 to 10,000, the worst-case time-delay margin decreases from 0.062 to 0.022 (i.e., about three times). However, for $C_1(s)$, it decreases from 0.17 to 0.15 (i.e., only 1.2 times). Thus, with a smaller choice of Γ, $C_1(s)$ is more suitable in terms of robustness as compared with $C(s)$. Table 3 summarizes the margins for $C_1(s)$ with $\Gamma = 10,000$.

Finally, we simulate the system with increased control effectiveness reduction (50% of each surface) without any delays to test robustness of the $\mathcal{L}_1$ adaptive control scheme toward a different class of uncertainty. Figure 10 plots the vertical acceleration command tracking in the presence of the pitch break uncertainty and 50% reduction of control effectiveness for each actuator channel. We see that the $\mathcal{L}_1$ adaptive control architecture retains both its tracking property and worst time-delay margin of 0.20, as predicted by the $\mathcal{L}_1$ theory. In Table 4, we have summarized the worst-case time-delay margins for two cases of control effectiveness reduction.

Table 1 Phase and time-delay margins for the inner loop

Loop margin	$\dot{p}$	$\dot{q}$	$\dot{r}$
Phase margin, deg	85.6	65.6	66.1
Crossover frequency, rad/s	4.25	6.01	4.27
Time-delay margin, s	0.3515	0.1905	0.2702

Table 2 Time-delay margin for $\mathcal{L}_1$ for $C(s) = 1/(0.05s+1)$

$\dot{p}$	$\dot{q}$	$\dot{r}$	Number of loops
N/A	0.062	N/A	Individual
0.073	N/A	N/A	Individual
N/A	N/A	0.065	Individual
0.062	0.062	N/A	Two loops
N/A	0.065	0.065	Two loops
0.067	N/A	0.067	Two loops
0.062	0.062	0.062	Simultaneous

VI. Aerial Refueling

In this section, we apply the $\mathcal{L}_1$ adaptive controller to the AAR autopilot design. The probe-and-drogue refueling procedure is

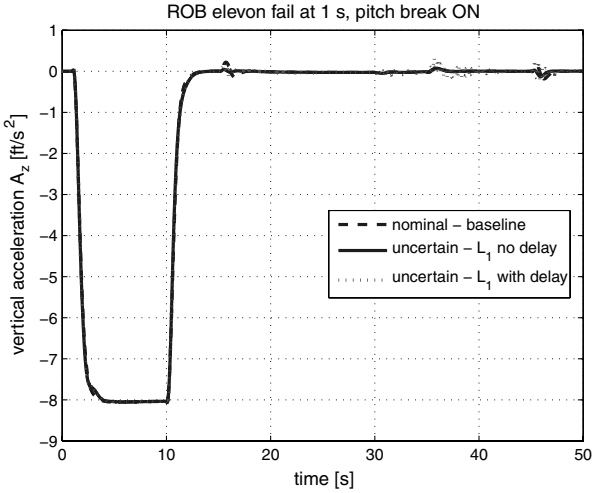

Fig. 6 Zoomed subplot of A_z (with time delay) (ROB denotes right outer board).

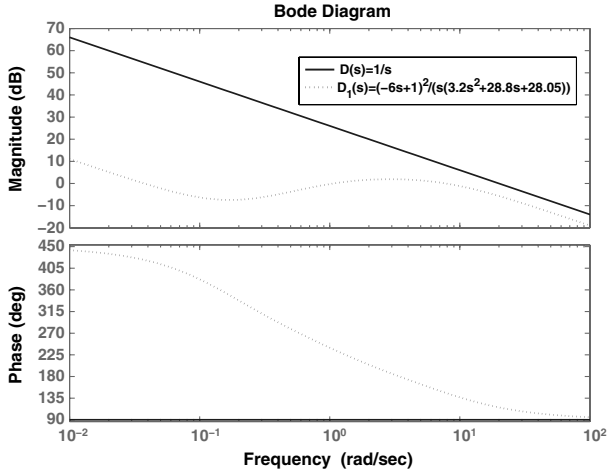

Fig. 7 Choice of $C(s)$ to maximize the time-delay margin.

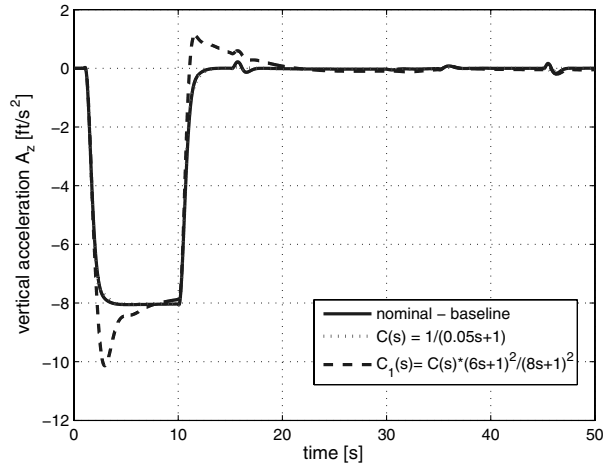

Fig. 8 Inner-loop adaptation with control effectiveness reduction and pitch break phenomenon [command tracking for different choice of $C(s)$].

adopted. This has proven to be extremely difficult, due to the aerodynamic coupling among the two aircraft, the receiver and the tanker, and the drogue. The autopilot has to compensate for the uncertainties, due to the trailing vortices of the tanker when the receiver is flying from the observation point to the contact point. As compared with the earlier work of the authors [19], the control signal, defined via the equations (27), (28), and (30) subject to the

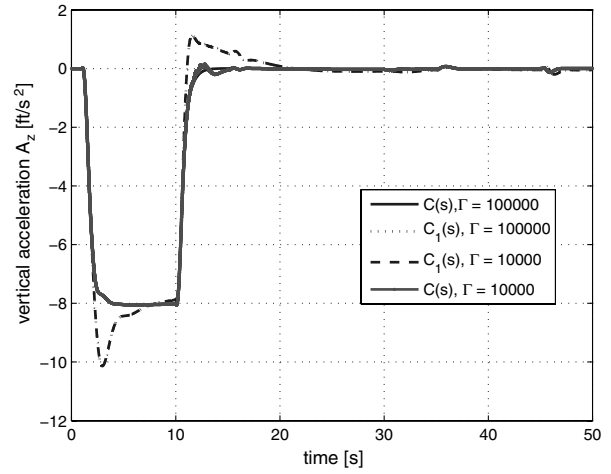

Fig. 9 Inner-loop adaptation with control effectiveness reduction and pitch break phenomenon (command tracking for different values of Γ).

Table 3 Time-delay margin of $\mathcal{L}_1$ for $C_1(s)$ and $\Gamma = 10,000$

$\dot{p}$	$\dot{q}$	$\dot{r}$	Number of loops
N/A	0.15	N/A	Individual
0.24	N/A	N/A	Individual
N/A	N/A	0.25	Individual
0.15	0.15	N/A	Two loops
N/A	0.15	0.15	Two loops
0.17	N/A	0.17	Two loops
0.15	0.15	0.15	Simultaneous

$\mathcal{L}_1$-norm upper bound in Eq. (26), eliminates the need for selecting and tuning basis functions required by the neural-network-based $\mathcal{L}_1$ adaptive control. This reduces the design effort significantly.

We consider a decoupled linearized six-degree-of-freedom aircraft model for the receiver aircraft. Both the receiver and the tanker aircraft are in straight and level flight in the beginning of the maneuver. The receiver is assumed to be subject only to small perturbations during the entire refueling maneuver, so that the linearized decoupled dynamics can be used to describe its motion with some level of fidelity (with additive uncertainties coming from the trailing vortices induced by the tanker aircraft). For the aerial refueling maneuver, all angles are assumed small. Despite these assumptions, we also neglect the direct influence of gravity, thrust, and elevator on the AOA. The drogue position is known and served as reference command $z_c(t)$, and the control objective is to fly the receiver into a prescribed neighborhood of the drogue center within a prescribed finite time interval. Upon incorporating the inner-loop baseline controllers into the system dynamics, the system to be controlled has three inputs: thrust, elevator, and aileron, and it has three outputs: horizontal separation, vertical separation, and lateral separation relative to the tanker. The control objective is to regulate the three outputs to certain set points in the presence of aerodynamic uncertainties (drag, pitching moment, and rolling moments) in three directions, respectively, and in the presence of control surface failures.

The aircraft model is a flying wing unmanned aerial vehicle (UAV), known as the Barron Associates' nonlinear tailless aircraft model [15]. The wake effect data which model the vortex are taken from a wind-tunnel test of a delta wing UAV behind a KC-135R tanker [20]. The baseline controller is a linear quadratic regulation (LQR) controller with integral action. For this LQR + PI (proportional integral) controller structure, the feedforward gain K_z is zero. The system takes the form in Eq. (16), which is repeated here for the sake of completeness:

$$\dot{x}(t) = A_m x(t) + B_m z_c(t) + B_1\{\Lambda u_{\text{ad}}(t) + \Lambda K_0[t,\, x_p(t)] + k_x^{\top} x(t)\} \tag{63}$$

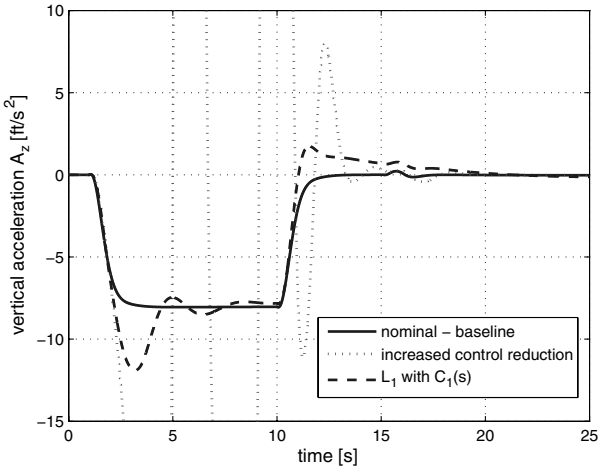

Fig. 10 Baseline controller almost loses stability in the presence of increased control reduction, whereas $\mathcal{L}_1$ proves guaranteed tracking.

Table 4 Worst-case time-delay margin with 30 and 50% control effectiveness reduction

30% case	50% case	Low-pass filter	Γ
0.062	0.071	$C(s)$	100,000
0.022	0.025	$C(s)$	10,000
0.17	0.20	$C_1(s)$	100,000
0.15	0.20	$C_1(s)$	10,000

where $x(t) \in \mathbb{R}^{14}$, $u_{\text{ad}}(t) \in \mathbb{R}^3$ (thrust, elevator, and aileron), and $z_c(t) \in \mathbb{R}^3$ are the measured system states, control signals, and reference inputs, respectively, and $A_m \in \mathbb{R}^{14\times14}$, $B_m \in \mathbb{R}^{14\times3}$, and $B_1 \in \mathbb{R}^{14\times3}$ are the known matrices for which the three columns of B_1 are linearly independent. The definitions of Λ and k_x are given in Eq. (17). Notice that there is no k_z in Eq. (63). The state vector $x = (l, V, \alpha, \theta, q, h, \phi, \beta, p, r, y, l_I, h_I, y_I)^\top$ comprises 11 plant states x_p, which include horizontal separation l, velocity V, AOA α, pitch angle θ, pitch rate q, vertical separation h, roll angle ϕ, angle of side slip β, body roll rate p, body yaw rate r, lateral separation y, and three baseline controller x_c states, which include integrator states of separation (l_I, h_I, and y_I). The simulation results and the $\mathcal{L}_1$ controller parameters are given in this section. More details of system dynamics and baseline controllers can be found in [19].

The target point for the receiver aircraft is chosen to be the center of the outer cross section of the drogue. The aircraft is trimmed at a speed of $V_0 = 500$ ft/s, and AOA of $\alpha_0 = 0.042$ rad, a pitch angle of $\theta_0 = 0.042$ rad, and at the altitude of $h = 5000$ ft. The radius of the drogue is $r_d = 1$ ft. The initial position of the receiver aircraft is 165 ft behind the tanker, 50 ft below the tanker, and 10 ft to the left of the aircraft, laterally. Relative to the tanker coordinate system, the position of the drogue center is at the coordinates $x_d = -15$ ft, $y_d = 30$ ft, and $z_d = 10$ ft.

The closed-loop system with these baseline controller gains defines the nominal linear system response that has the desired convergence time for the probe to contact the drogue with the desired performance specifications. The adaptive augmentation with the $\mathcal{L}_1$ controller is designed to track this system's response both in the transient and steady states. In the absence of wake-induced uncertainties and without any loss in control effectiveness, the probe reaches the 0.02 ft neighborhood of the drogue center within 25 s. That is, $|x(25) - x_d(25)| = 0.012$, $|y(25) - y_d(25)| = 0.015$ and $|z(25) - z_d(25)| = 0.02$. Figure 11 plots the closed-loop trajectories in each axis. It compares the responses in the absence of the wake and without any loss in control effectiveness to the response in the presence of the wake and loss in control effectiveness. The failures are a 60% reduction of elevator effectiveness, and a 60% reduction of

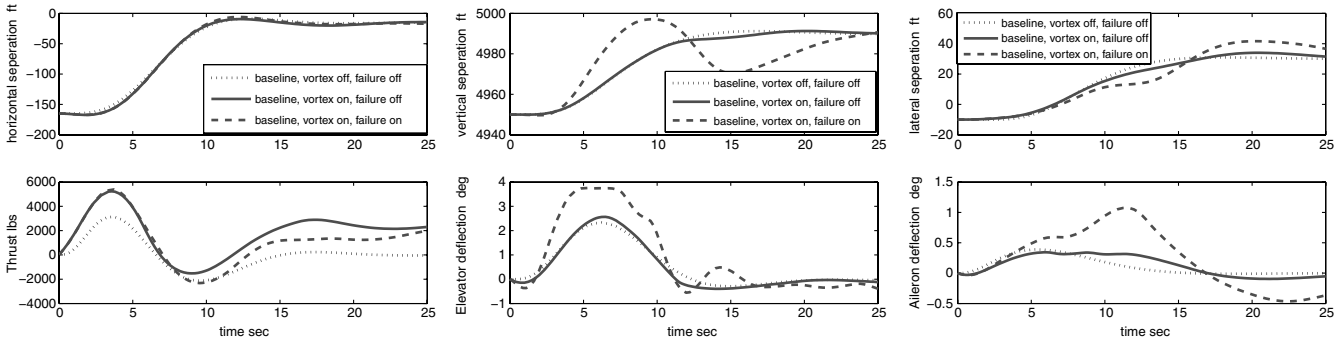

Fig. 11 Horizontal, vertical, and lateral separations (baseline controller).

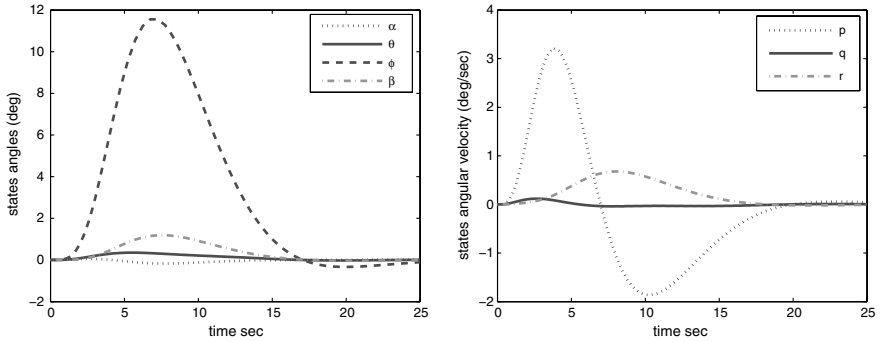

Fig. 12 Angles and angular velocities (baseline controller).

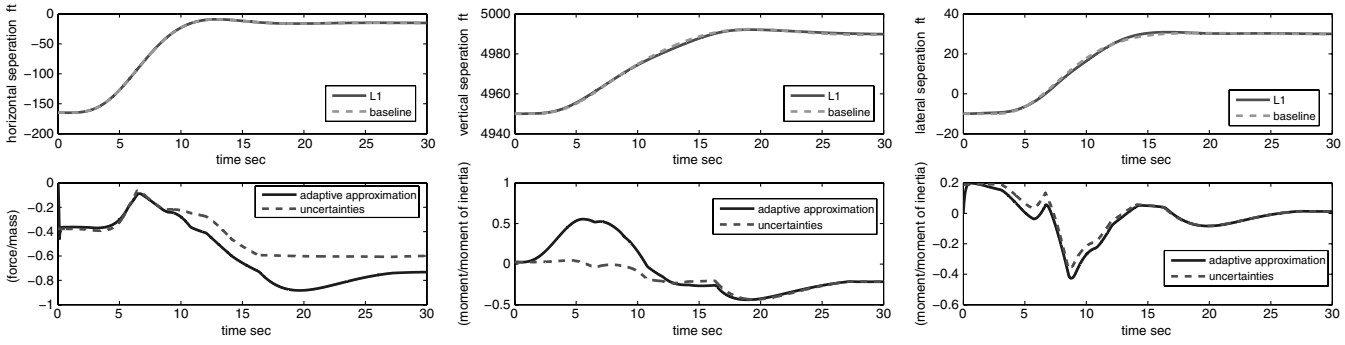

Fig. 13 Horizontal, vertical, and lateral separation baseline + $\mathcal{L}_1$ controllers.

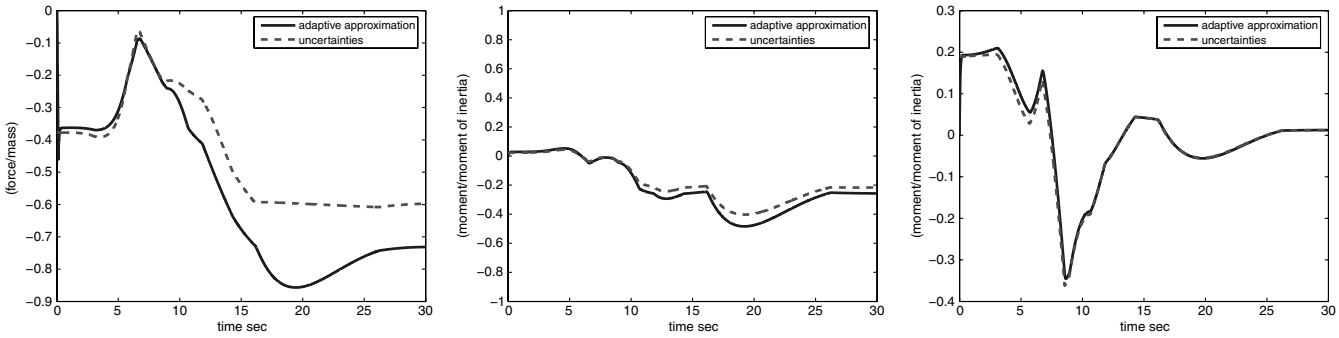

Fig. 14 $\mathcal{L}_1$ adaptive control signals and uncertainties (failure off).

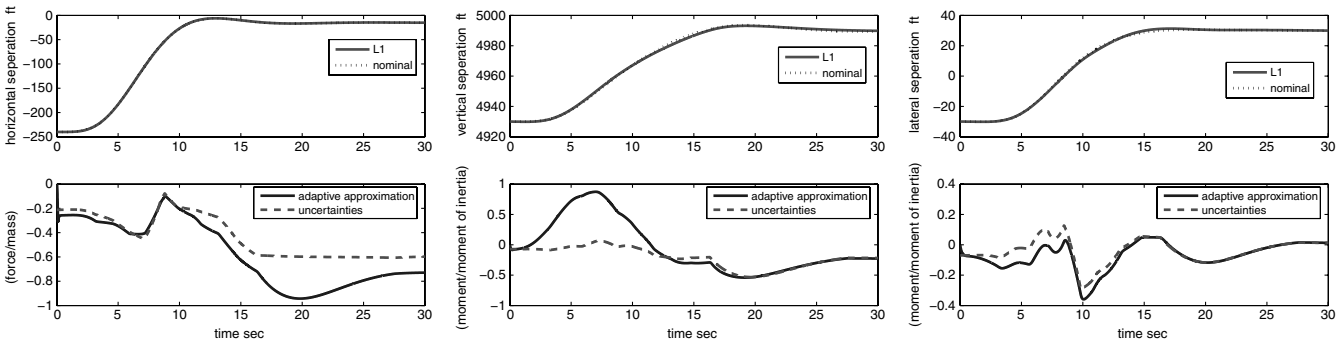

Fig. 15 Horizontal, vertical, and lateral separation (second case).

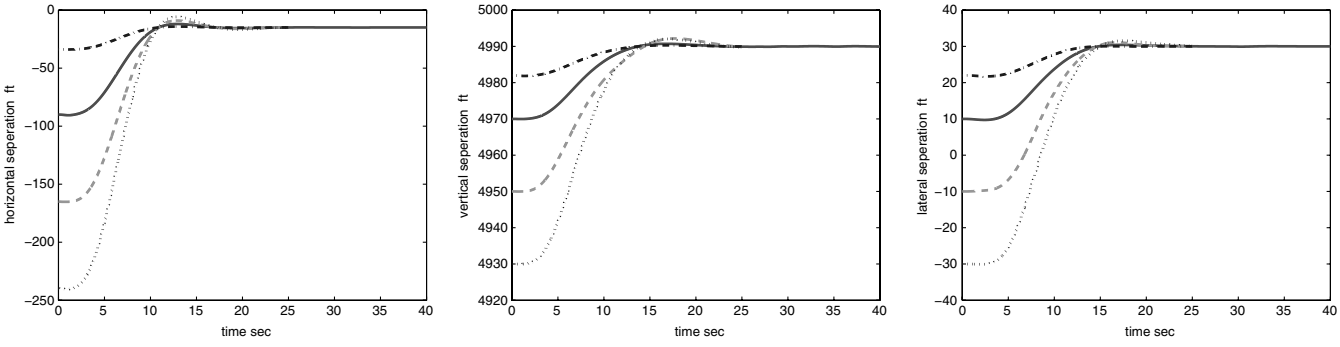

Fig. 16 Horizontal, vertical, and lateral separation (scaled responses).

aileron effectiveness (that is, $\Lambda_2 = \Lambda_3 = 0.4$). From these figures, we can see that both the steady-state tracking and the transient performance are deteriorated in the presence of the uncertainties. Figure 12 shows the other states (AOA α, pitch angle θ, roll angle ϕ, side-slip angle β, roll rate p, pitch rate q, and yaw rate r) of the baseline controlled closed-loop system. Those states remain small during the whole aerial refueling process.

For the design of the $\mathcal{L}_1$ controller, we choose $D_i(s) = \frac{1}{s}$, $i = 1, \cdots, m$. Conservative growth rates for the uncertainties are computed from the experimental data, implying that $\max L_{w_i} = 0.1$. The conservative maximum is given by $L_i = 10.1$. We choose $k_1 = k_2 = k_3 = 20$, leading to $C_1(s) = 20/(s + 20)$, $C_2(s) = 8/(s + 8)$, and $C_3(s) = 8/(s + 8)$. We set a uniform adaptive gain of $\Gamma = 100,000$ for the design of the adaptive controller in each axis.

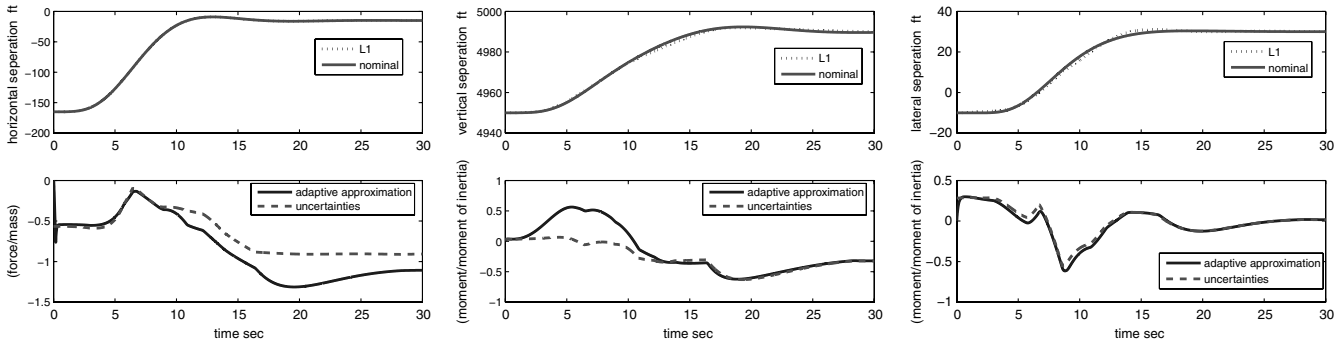

Fig. 17 Horizontal, vertical, and lateral separation (increased vortex magnitude).

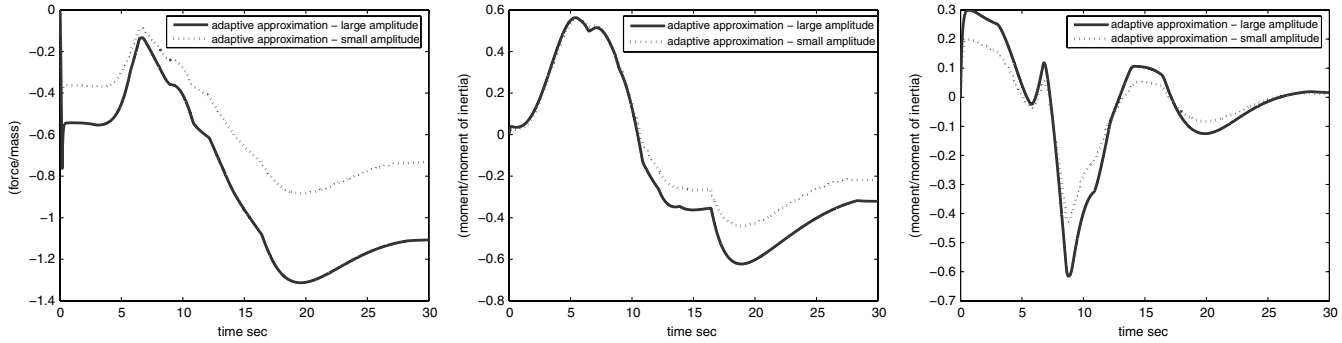

Fig. 18 Adaptive signals vs uncertainties (increased vortex magnitude).

The closed-loop system response with the $\mathcal{L}_1$ adaptive augmentation and the adaptive control signals are shown in Fig. 13. We notice that the $\mathcal{L}_1$ adaptive controller can recover the nominal performance of the baseline controller in the presence of the wake vortex and the loss in control effectiveness. The tracking precision upon $t' = 25$ s can be characterized with the bound $\| [y(t') \quad z(t')]^\top - [y_d(t') \quad z_d(t')]^\top \| = 0.05 \leq 1$ and $|x(t') - x_d(t')| = 0.04$. Notice that in the thrust input channel, at the steady state, there is a difference between the time histories of the adaptive approximation and the uncertainty. That is caused by the residue of the elevator control input coming into the horizontal direction. In the elevator and aileron plots, we see that there are some differences between the adaptive signals and the uncertainties during the transient phase. If we turn off the actuator failure, the adaptive approximation will be much closer to the uncertainties, as shown in Fig. 14.

Next, we show that when the initial conditions change, the $\mathcal{L}_1$ controller does not need any retuning.

We change the initial conditions of the receiver. We keep the same values for Λ_1 and Λ_2 and run the simulations from 33.75 ft behind the tanker, 18 ft below the tanker, and 22 ft to the right of the tanker without any retuning of both controllers. The $\mathcal{L}_1$ adaptive controller achieves the tracking precision upon $t' = 25$ s, which is $\| [y(t') \quad z(t')]^\top - [y_d(t') \quad z_d(t')]^\top \| = 0.021 \leq 1$ and $|x(t') - x_d(t')| = 0.020$, as in Fig. 15. We observe that the $\mathcal{L}_1$ adaptive controller shows scaled system output responses (similar to linear systems).

Without retuning of the $\mathcal{L}_1$ controller, we further run the simulations, starting from various different initial conditions, as shown in Fig. 16. It can be seen that the system outputs have scaled responses. We further increase the uncertainties by multiplying the magnitude of the vortex data by two. This can approximately represent a different tanker if we consider a modified horseshoe vortex model. With fixed separations between the receiver and the tanker, the magnitude of the induced velocity is proportional to the strength of the vortex, which is, in its turn, proportional to the mean aerodynamic chord of the tanker and the velocity of the tanker. And so, it is reasonable to scale our current induced aerodynamic coefficients by multiplying them by two to represent the change of tanker's wake effects. Figure 17 shows that the outputs are identical to the nominal performance, and Fig. 18 shows that the adaptive control signals have scaled responses corresponding to the change of the uncertainties.

Finally, we compute the time-delay margin of the $\mathcal{L}_1$ adaptive controlled system similar to the UCAV model previously described. First, we use the low-pass filters $C_2(s) = C_3(s) = 25/(s + 25)$. The numerical values are shown in Table 5.

We next change the low-pass filter to $C_2(s) = C_3(s) = 8/(s + 8)$. The time-delay margins are given in Table 6.

We see that, by tuning the phase margin of $C(s)$, we can improve the time-delay margin of the $\mathcal{L}_1$ adaptive control system. This verifies the theoretical claims.

Table 5 Time-delay margin of $\mathcal{L}_1$ for $C_2(s) = C_3(s) = 25/(s + 25)$ and $\Gamma = 100,000$

Elevator	Aileron	Number of loops
0.028	N/A	Individual
N/A	0.031	Individual
0.028	0.030	Simultaneous

Table 6 Time-delay margin of $\mathcal{L}_1$ for $C_2(s) = C_3(s) = 8/(s + 8)$ and $\Gamma = 100,000$

Elevator	Aileron	Number of loops
0.042	N/A	Individual
N/A	0.081	Individual
0.041	0.080	Simultaneous

VII. Conclusions

The $\mathcal{L}_1$ adaptive controller is applied to two benchmark flight control applications in this paper. The proposed adaptive control approach overcomes the drawbacks of conventional adaptive control methods. It has guaranteed performance bounds and systematic design methodology to achieve the desired control specifications. The bounded-away-from-zero time-delay margin of this adaptive controller can be improved by the systematic choice of the underlying filters. These features hold a promise for the development of theoretically justified tools for VV of the adaptive systems. Future work will address the design of the low-pass filter for achieving the desired tradeoff for a broader class of systems.

Appendix

We recall some definitions and facts from linear systems theory [21–23].

Definition 1: For a signal $\xi(t)$, $\xi \in \mathbb{R}^n$, its truncated $\mathcal{L}_\infty$ norm, and $\mathcal{L}_\infty$ norm are defined as

$$\|\xi_t\|_{\mathcal{L}_\infty} = \max_{i=1,\ldots,n} \left(\sup_{0 \leq \tau \leq t} |\xi_i(\tau)| \right)$$

$$\|\xi\|_{\mathcal{L}_\infty} = \max_{i=1,\ldots,n} \left(\sup_{\tau \geq 0} |\xi_i(\tau)| \right)$$

where ξ_i is the ith component of ξ.

Definition 2: The $\mathcal{L}_1$ norm of a stable proper single-input–single-output system $H(s)$ is defined to be

$$\|H(s)\|_{\mathcal{L}_1} = \int_0^\infty |h(t)| \, \mathrm{d}t$$

where $h(t)$ is the impulse response of $H(s)$.

Definition 3: For a stable proper m-input–n-output system $H(s)$, its $\mathcal{L}_1$ norm is defined as

$$\|H(s)\|_{\mathcal{L}_1} = \max_{i=1,\cdots,n}\left(\sum_{j=1}^{m}\|H_{ij}(s)\|_{\mathcal{L}_1}\right)$$

where $H_{ij}(s)$ is the ith row jth column element of $H(s)$.

Acknowledgments

This material is based upon work supported by the U.S. Air Force (under contract nos. FA8650-05-C-3563, FA9550-05-1-0157, FA 9550-08-1-0135) and NASA (under contract nos. NNX08 AB97A, NNX08AC81A). Any opinions, findings, and conclusions or recommendations expressed in this material are those of the authors and do not necessarily reflect the views of the U.S. Air Force or NASA. The authors are thankful to Kevin Wise and Eugene Lavretsky from The Boeing Company for their help with the simulation models and the historical overview of adaptive flight control, summarized in the introduction.

References

[1] Sharma, M., Calise, A. J., and Corban, J. E., "Application of an Adaptive Autopilot Design to a Family of Guided Munitions," AIAA Guidance, Navigation, and Control Conference and Exhibit, AIAA Paper 2000-3969, Aug. 2000.

[2] Calise, A. J., Sharma, M., and Corban, J. E., "Adaptive Autopilot Design for Guided Munitions," *Journal of Guidance, Control, and Dynamics*, Vol. 23, No. 5, 2000.

[3] Sharma, M., Wise, K., and Lavretsky, E., "Application and Flight Testing of an Adaptive Autopilot on Precision Guided Munitions," AIAA Guidance, Navigation, and Control Conference and Exhibit, AIAA Paper 2006-6568, Aug. 2006.

[4] Wise, K., Lavretsky, E., Zimmerman, J., Francis, J., Jr., Dixon, D., and Whitehead, B., "Adaptive Flight Control of a Sensor Guided Munition," AIAA Guidance, Navigation, and Control Conference and Exhibit, AIAA Paper 2005-6385, Aug. 2005.

[5] Wise, K., "Reconfigurable Systems for Tailless Fighter Aircraft: RESTORE," U.S. Air Force Research Laboratory Final Rept. VA-WP-TR-99-3067, 1999.

[6] Wise, K., and Brinker, J., "Reconfigurable Flight Control for a Tailless Advanced Fighter Aircraft," AIAA Guidance, Navigation, and Control Conference and Exhibit, AIAA Paper 1998-4107, Aug. 1998.

[7] Wise, K., Brinker, J., Calise, A., Enns, D., Elgersma, M., and Voulgaris, P., "Direct Adaptive Reconfigurable Flight Control For A Tailless Advanced Fighter Aircraft," *International Journal of Robust and Nonlinear Control*: Special Issue on Reconfigurable Flight Control, Vol. 9, No. 14, 1999, pp. 999–1012. doi:10.1002/(SICI)1099-1239(19991215)9:14<999::AID-RNC449>3.0.CO;2-O

[8] Wise, K., Lavretsky, E., and Hovakimyan, N., "Adaptive Control of Flight: Theory, Applications, and Open Problems," *Proceedings of the American Control Conference*, IEEE Publications, Piscataway, NJ, June 2006. doi:10.1109/ACC.2006.1657677

[9] Cao, C., and Hovakimyan, N., "Design and Analysis of a Novel $\mathcal{L}_1$ Adaptive Control Architecture with Guaranteed Transient Performance," *IEEE Transactions on Automatic Control*, Vol. 53, No. 2, 2008, pp. 586–891. doi:10.1109/TAC.2007.914282

[10] Cao, C., and Hovakimyan, N., "Stability Margins of $\mathcal{L}_1$ Adaptive Controller: Part 2," *Proceedings of the American Control Conference*, IEEE Publications, Piscataway, NJ, July 2007, pp. 3931–3936.

[11] Cao, C., and Hovakimyan, N., "$\mathcal{L}_1$ Adaptive Controller for a Class of Systems with Unknown Nonlinearities: Part 1," *Proceedings of the American Control Conference*, IEEE Publications, Piscataway, NJ, 2008, pp. 4093–4098.

[12] Cao, C., and Hovakimyan, N., "Adaptive Output Feedback Controller for Systems of Unknown Dimension," *IEEE Transactions on Automatic Control*, Vol. 53, No. 3, 2008, pp. 815–821. doi:10.1109/TAC.2008.919550

[13] Cao, C., and Hovakimyan, N., "Novel $\mathcal{L}_1$ Neural Network Adaptive Control Architecture with Guaranteed Transient Performance," Special Issue on Feedback Control of *IEEE Transactions on Neural Networks*, Vol. 18, No. 4, 2007, pp. 1160–1171. doi:10.1109/TNN.2007.899197

[14] Cao, C., Hovakimyan, N., "Guaranteed Transient Performance with $\mathcal{L}_1$ Adaptive Controller for Systems with Unknown Time-Varying Parameters and Disturbances in the Presence of Non-Zero Trajectory Initialization Error," *International Journal of Control*, Vol. 81, No. 7, 2008, pp. 1147–1161. doi:10.1080/00207170701670939

[15] Farrell, J., Sharma, M., and Polycarpou, M., "Backstepping-Based Flight Control with Adaptive Function Approximation," *Journal of Guidance, Control, and Dynamics*, Vol. 28, No. 6, 2005, pp. 1089–1102. doi:10.2514/1.13030

[16] Li, D., Hovakimyan, N., Cao, C., and Wise, K., "Filter Design for Feedback-Loop Trade-Off of $\mathcal{L}_1$ Adaptive Controller: A Linear Matrix Inequality Approach," AIAA Guidance, Navigation, and Control Conference, AIAA Paper 2008-6280, Aug. 2008.

[17] Patel, V., Cao, C., Hovakimyan, N., Wise, K., and Lavretsky, E., "$\mathcal{L}_1$ Adaptive Controller for Tailless Unstable Aircraft in the Presence of Unknown Actuator Failures," *International Journal of Control*, Vol. 82, No. 4, 2009, pp. 705–720. doi:10.1080/00207170802225955

[18] Li, D., Hovakimyan, N., and Cao, C., "$\mathcal{L}_1$ Adaptive Controller in the Presence of Input Saturation," AIAA Guidance, Navigation, and Control Conference, AIAA Paper 2009-6064, Aug. 2009.

[19] Wang, J., Patel, V., Cao, C., Hovakimyan, N., and Lavretsky, E., "Novel $\mathcal{L}_1$ Adaptive Control Methodology for Aerial Refueling with Guaranteed Transient Performance," *Journal of Guidance, Control, and Dynamics*, Vol. 31, No. 1, 2008, pp. 182–193. doi:10.2514/1.31199

[20] Blake, W. B., Dickes, E. G., and Gingras, D. R., "UAV Aerial Refueling: Wind Tunnel Results and Comparison with Analytic Predictions," AIAA Atmospheric Flight Mechanics Conference and Exhibit, AIAA Paper 2004-4820, 2004.

[21] Ioannou, P., and Sun, J., *Robust Adaptive Control*, Prentice–Hall, Englewood Cliffs, NJ, 1996.

[22] Khalil, H. K., *Nonlinear Systems*, Prentice–Hall, Englewood Cliffs, NJ, 2002.

[23] Zhou, K., and Doyle, J. C., *Essentials of Robust Control*, Prentice–Hall, Englewood Cliffs, NJ, 1998.